International Journal of Electrical, Electronic and Communication Sciences
ISSN: 2517-9438
Vol:7, No:11, 2013

A New Self-Tuning Fuzzy PD Controller of a BDFIG for Wind Energy Conversion

Zoheir Tir, Rachid Abdessemed

***Abstract*—**This paper presents a new control scheme to control a brushless doubly fed induction generator (BDFIG) using back-to-back PWM converters for wind power generation. The proposed control scheme is a New Self-Tuning Fuzzy Proportional-Derivative Controller (NSTFPDC). The goal of BDFIG control is to achieve a similar dynamic performance to the doubly fed induction generator (DFIG), exploiting the well-known induction machine vector control philosophy. The performance of NSTFPDC controller has been investigated and compared with the two controllers, called Proportional–Integral (PI) and PD-like Fuzzy Logic controller (PD-like FLC) based BDFIG. The simulation results demonstrate the effectiveness and the robustness of the NSTFPDC controller.

***Keywords*—**Brushless Doubly Fed Induction Generator (BDFIG), PI controller, PD-like Fuzzy Logic controller, New Self-Tuning Fuzzy Proportional-Derivative Controller (NSTFPDC), Scaling factor, back-to-back PWM converters, wind energy system.

I. Introduction

DURING the last years, the use of wind energy generation industry has been growing rapidly [1]. This is due to the fact that this energy source production of electricity is emission free [1], [2]. Currently, the Brushless Doubly Fed Induction Generator (BDFIG) promises significant advantages for wind power applications [3]-[9]. The use of the BDFIG, however, decreased the cost and complexity of the wind turbines due to the absence of the slip ring system and simpler structure of the rotor winding [3]-[10]. A typical configuration of a BDFIG wind turbine is shown schematically in Fig. 1.

A BDFIG is composed of two stator windings with different pole numbers (called power winding (PW) and control winding (CW)) and a special rotor winding [5], [8], [9]. However, it allows putting a converter between the CW and the grid which is designed only for a part of the full power of the machine (about 30 %) [3], [10]. By controlling correctly this converter, variable-speed operation is allowed and electrical power can be produced from the PW to the grid and also from the CW to the grid. Direct magnetic field coupling does not exist between the PW and CW, and the electromechanical energy conversion is realized by the magnetic field modulation of the rotor winding [3], [10].

Z. Tir is with the Department of Electrical Engineering, university of Eloued, B.P.789, 39000, El-Oued, Algeria (phone: 213 662 730 917; e-mail: tir-zoheir@univ-eloued.dz).

R. Abdessemed is with the Department of Electrical Engineering, university of Batna,05000 Batna, Algeria (e-mail: r.abdessemed@lycos.com).

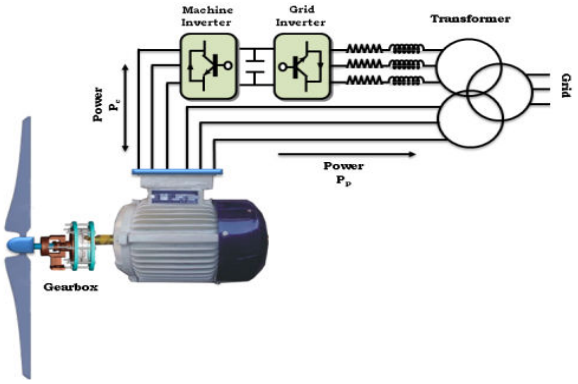

Fig. 1 BDFIG Configuration for Wind Power Generation

In this paper presents a new control scheme to control a BDFIG. The proposed control scheme, called "a New Self-Tuning Fuzzy PD Controller (NSTFPDC)". In comparison with two different controllers: Proportional-Integral (PI) and PD-type Fuzzy Logic (PD-type FLC). PI and PD-type FLC have a proven control performance for many industrial drives [11]-[16]. A PI controller can compensate machine variations very efficiently via the appropriate tuning of its dominant parameters [15]. However, the performance may significantly deteriorate when the operating condition is changed or when the parameters drift [15], [16], a PD-type FLC has been found particularly suitable for controller design when the machine is difficult to model mathematically due to its complexity, nonlinearity [11]-[19]. It might help reduce hardware and cost and provide better performance than the PI controller [12]-[16]. On the other hand, the performance of the PD-type FLC may not offer the required control action. Such PD-type FLC with fixed values of scaling factors is not expected to present good control performance [14]-[16]. Several attempts have been made to enhance the self-adaptability and performance of the PD-type FLC is scaling factor (SF) tuning; it has a significant impact on the performance of a PD-type FLC [14]-[16].

Some works on PD-type FLC tuning have also been done with the implementation of genetic algorithms or neural networks to minimize overshoot, settling time, and rising time [14]-[16]. As the authors, Mudi and Pal [14], [16] proposed a robust self-tuning fuzzy PD-type controller (STFPDC). However, the major disadvantage of the control scheme, its value of the scaling factor of fuzzy output (α) is obtained by 49 fuzzy rules defined on error (e) and change error (ce), this will require us a high speed microprocessor in order to obtain good results, this also is what makes the expensive device

[16]. To cure this problem, we propose a new control scheme to control a BDFIG, called "a New Self-Tuning Fuzzy Proportional-Derivative Controller (NSTFPDC)" its output SF is continuously modified by a single deterministic rule defined on the normalized of error (e) and change error (ce). The role of the proposed heuristic rule is expected to improve the performance of the BDFIG in terms of reference tracking, sensibility to perturbations and parameters variations.

Depending on the values of the average (steady state) wind speed, four zones may be identified in the static operation of BDFIG [1], [2], [20]. Zones I and VI, where the provided power is zero, are not concerned by this paper. The interest is here focused on zone II, called partial load zone, where the extracted power proportionally depends on the wind speed cubed.

II. Modeling of the Wind Turbine and Gearbox

The theoretical power available in the wind is defined by Betz formula. It is given by

$$P_w = \frac{1}{2} \cdot \rho \cdot S \cdot v_w^3 \quad (1)$$

All this power is not recovered on the shaft of the turbine depending on the geometry of the turbine and frictions [1], [20], [2].

The effective efficiency conversion is given by the power coefficient (Cp), which is expressed by the following:

$$C_p = \frac{P_t}{P_w} \quad (2)$$

where P_t is the mechanical power of the turbine and P_w is the available wind power.

The relative speed λ is defined as the ratio between blade tip speed and wind speed; it is expressed as:

$$\lambda = \frac{\Omega_t R}{V_w} \quad (3)$$

A typical relationship between C_p and λ is shown in Fig. 2. It is clear from this figure that there is a value of λ for which C_p is maximum and that maximize the power for a given wind speed. The peak power for each wind speed occurs at the point where C_p is maximized. To maximize the generated power, it is therefore desirable for the generator to have a power characteristic that will follow the maximum C_{p_max} [20].

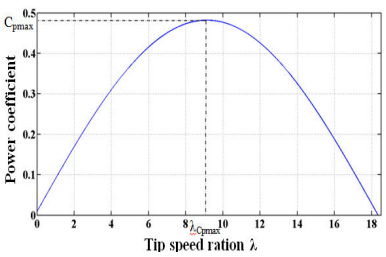

Fig. 2 Power coefficient for the wind turbine model

Taking into account (1)-(3), power on the out axle of the turbine is then:

$$P_t = \frac{1}{2}.C_p.\rho.\pi.R^5.\frac{\Omega_t}{\lambda^3} \quad (4)$$

Torque is then:

$$C_t = \frac{P_t}{\Omega_t} \quad (5)$$

$$C_{em} = \frac{P_t}{\Omega_t} = \frac{1}{2} \cdot \rho \cdot \pi \cdot R^3 \cdot C_p \cdot v_w^3 \quad (6)$$

With the multiplier of report/ratio G, the torque and speed become at shaft end;

$$C_g = \frac{C_t}{G} \text{ and } \Omega_t = \frac{\Omega_{mec}}{G} \quad (7)$$

When the turbine is coupled to a machine the mechanical equation at shaft end will be:

$$J\frac{d\Omega_{mec}}{dt} + f\Omega_{mec} = C_g - C_{em} \quad (8)$$

From these various equations the mathematical model of the turbine at shaft end is shown on Fig. 3.

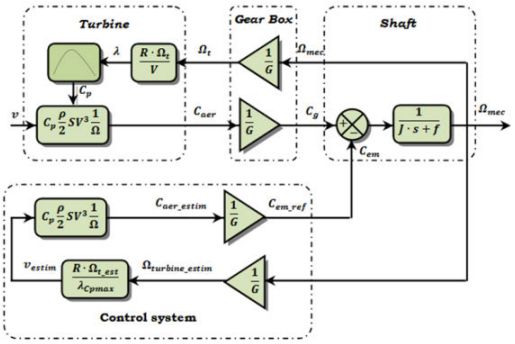

Fig. 3 Device control without control speed [2]

The expression of the optimal mechanical power P_{mec_opt} is obtained as follows:

$$P_{mec_{opt}} = \frac{1}{2}\frac{C_{pmax}.\rho.\pi.R^3}{G^3\lambda_{opt}^3} \cdot \Omega_{mec}^3 \quad (9)$$

III. BDFIG Operation and Dynamical Model

The stator of the BDFIG has two separate windings, namely, power winding (PW) and control winding (CW), with different pole pair numbers to avoid direct coupling between the windings (PW and CW) [3]-[7], [9]. A specially designed rotor is able to couple both the PW and CW [4], [5]. The PW is directly connected to the grid, where as the CW is connected to the grid through a bidirectional converter.

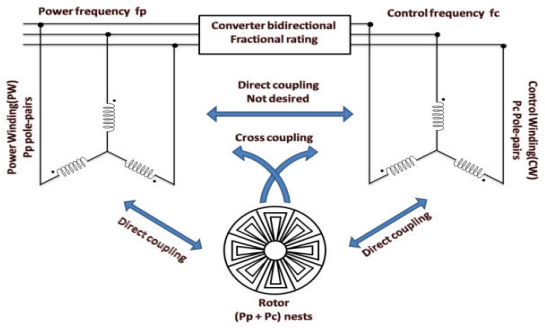

Fig. 4 The basic structure of BDFIG

In order to assure the related cross-coupling effect by the simplest machine structure the number of rotor loops (N_r) has to be selected as [3], [10]:

$$N_r = p_p + p_c \tag{10}$$

Direct coupling phenomena between the two stator windings must be prevented, so next supplementary restriction must be adopted [3], [7], [8].

$$p_p \neq p_c \tag{11}$$

In order to obtain the desired cross-coupling effect, the currents that both the PW and the CW induce at the rotor bars must evolve with the same frequency [3], [9]. The synchronous rotor speed ω_r is determined by the excitation frequencies of two stator windings, as expressed by

$$\omega_r = \frac{\omega_p + \omega_c}{p_p + p_c} \tag{12}$$

Because of that a synchronization procedure is required in the start up phase. Once the synchronous operation mode is reached, the BDFIG shows a stable behavior, and then the rotor speed can be easily controlled by ω_c [8], [9], [4]-[6].

When the CW angular frequency ω_c is equal to zero, the angular frequency of the rotor is defined as the natural angular frequency ω_n, as expressed by [5], [6], [9]

$$\omega_n = \frac{\omega_p}{p_p + p_c} \tag{13}$$

In this paper, the pole-pair numbers of the PW and CW are one and three [7], [8], [10], respectively, and the grid frequency is 50 Hz. Thus, the natural synchronous speed is equal to 750 rmp.

The electrical equations used to model the BDFIG in the Park reference frame are [7]:

$$v_{sp}^q = R_{sp} i_{sp}^q + \frac{d\psi_{sp}^q}{dt} + \omega_p \psi_{sp}^d \tag{14}$$

$$v_{sp}^d = R_{sp} i_{sp}^d + \frac{d\psi_{sp}^d}{dt} - \omega_p \psi_{sp}^q \tag{15}$$

$$0 = R_r i_r^q + \frac{d\psi_r^q}{dt} + (\omega_p - p_p \omega_r)\psi_r^d \tag{16}$$

$$0 = R_r i_r^d + \frac{d\psi_r^d}{dt} - (\omega_p - p_p \omega_r)\psi_r^q \tag{17}$$

$$v_{sc}^q = R_{sc} i_{sc}^q + \frac{d\psi_{sc}^q}{dt} + (\omega_p - (p_p + p_c)\omega_r)\psi_{sc}^d \tag{18}$$

$$v_{sc}^d = R_{sc} i_{sc}^d + \frac{d\psi_{sc}^d}{dt} - (\omega_p - (p_p + p_c)\omega_r)\psi_{sc}^q \tag{19}$$

The expressions for stators and rotor flux linkages are [7]

$$\psi_{sp}^q = L_{sp} i_{sp}^q + L_{mp} i_r^q \tag{20}$$

$$\psi_{sp}^d = L_{sp} i_{sp}^d + L_{mp} i_r^d \tag{21}$$

$$\psi_r^q = L_{mp} i_{sp}^q + L_r i_r^q + L_{mc} i_{sc}^q \tag{22}$$

$$\psi_r^d = L_{mp} i_{sp}^d + L_r i_r^d + L_{mc} i_{sc}^d \tag{23}$$

$$\psi_{sc}^q = L_{sc} i_{sc}^q + L_{mc} i_r^q \tag{24}$$

$$\psi_{sc}^d = L_{sc} i_{sc}^d + L_{mc} i_r^d \tag{25}$$

The electromagnetic torque is [6]

$$C_{em} = \frac{3}{2}\left(p_p\left(\psi_{sp}^d i_{sp}^q - \psi_{sp}^q i_{sp}^d\right) + p_c L_{mc}\left(i_{sc}^d i_r^q - i_{sc}^q i_r^d\right)\right) \tag{26}$$

The active and reactive power at the stator as well as those provide for grid are defined as [1], [8], [9], [21], [22]

For PW are

$$\begin{cases} P_{sp} = \frac{3}{2}\left(v_{sp}^q i_{sp}^q + v_{sp}^d i_{sp}^d\right) \\ Q_{sp} = \frac{3}{2}\left(v_{sp}^q i_{sp}^d - v_{sp}^d i_{sp}^q\right) \end{cases} \tag{27}$$

For CW are:

$$\begin{cases} P_{sc} = \frac{3}{2}\left(v_{sc}^q i_{sc}^q + v_{sc}^d i_{sc}^d\right) \\ Q_{sc} = \frac{3}{2}\left(v_{sc}^q i_{sc}^d - v_{sc}^d i_{sc}^q\right) \end{cases} \tag{28}$$

IV. Field Oriented Control of a BDFIG

A. Reference-Frame

By choosing a reference frame linked to the PW flux, CW currents will be related directly to the PW active and reactive power. An adapted control of these currents will thus permit to control the power exchanged between the PW and the grid [8], [9]. If the PW flux is linked to the d-axis of the frame we have

$$\psi_{sp}^d = |\psi_{sp}| \; and \; \psi_{sp}^q = 0 \tag{29}$$

The obtained control strategy for the BDFIG is similar to the well-known stator field orientation control used in the DFIG [12].

B. Control Strategy

By aligning the d-axes with the flux vector of the power winding allows for the further simplification of (27). Therefore, as in (30) the active power flow of the BDFIG can be regulated through the q-component of the PW current.

$$\begin{cases} P_{sp} = \frac{3}{2} v_{sp}^{q}\, i_{sp}^{q} \\ Q_{sp} = \frac{3}{2} v_{sp}^{q}\, i_{sp}^{d} \end{cases} \quad (30)$$

The PW current can be expressed in terms of the rotor current and further CW stator current. Rearranging the PW stator flux and the rotor flux equations produces:

$$i_{sp} = \frac{\psi_{sp} - L_{mp} i_r}{L_{sp}} \quad (31)$$

$$i_r = \frac{\psi_r + L_{mp} i_r + L_{mc} i_{sc}}{L_r} \quad (32)$$

Then:

$$i_{sp} = \frac{L_r}{L_{sp}L_r - L_{mp}^2}\psi_{sp} - \frac{L_{mp}}{L_{sp}L_r - L_{mp}^2}\psi_r + \frac{L_{mc}L_{mp}}{L_{sp}L_r - L_{mp}^2} i_{sc} \quad (33)$$

Expanding (33) into d-q reference frame and substituting into (30) produces the expanded power flow expression for the BDFIG:

$$\begin{cases} P_p = \frac{3}{2} v_{sp}^{q} \left(\frac{L_{mp}}{L_{sp}L_r - L_{mp}^2}\psi_r^q - \frac{L_{mc}L_{mp}}{L_{sp}L_r - L_{mp}^2} i_{sc}^q \right) \\ Q_p = \frac{3}{2} v_{sp}^{q} \left(\frac{L_r}{L_{sp}L_r - L_{mp}^2}\psi_{sp}^d - \frac{L_{mp}}{L_{sp}L_r - L_{mp}^2}\psi_r^d + \frac{L_{mc}L_{mp}}{L_{sp}L_r - L_{mp}^2} i_{sc}^d \right) \end{cases} \quad (34)$$

The power terms in (34) are both expressed as a function of the CW stator current that can be directly controlled.

To begin the implementation of the power flow equations (34) in the controller, it is first necessary to trace the relationship between the current control signals of the CW and their equivalent voltage commands that can be utilized with the voltage source inverter:

$$v_{sc} = R_{sp}\, i_{sc} + \frac{d\psi_{sc}}{dt} + j\omega_c \psi_{sc} \quad (35)$$

The CW stator flux is estimated in (36). Rearranging the CW stator flux and expressing it in terms of some known quantities as well as rotor flux:

$$\psi_{sc} = \frac{L_{mc}L_{mp}}{L_r} i_{sp} - \frac{L_{mc}}{L_r}\psi_r + \frac{L_{sp}L_r - L_{mp}^2}{L_r} i_{sc} \quad (36)$$

For further simplification (33) can be substituted into (36), the result is then put into (35) and transformed into d-q frame:

$$\begin{cases} v_{sc}^d = R_{sc} i_{sc}^d + \frac{d}{dt}\left(\delta_3 i_{sc}^d + \delta_2 \psi_r^d - \delta_1 \psi_{sp}^d\right) - \omega_c\left(\delta_3 i_{sc}^q + \delta_3 \psi_r^q\right) \\ v_{sc}^q = R_{sc} i_{sc}^q + \frac{d}{dt}\left(\delta_3 i_{sc}^q + \delta_2 \psi_r^q\right) - \omega_c\left(\delta_3 i_{sc}^d + \delta_2 \psi_r^d - \delta_1 \psi_{sp}^d\right) \end{cases} \quad (37)$$

Thus, voltage expressions in (37) become the command signals to the controller of the VSI converter, shown in Fig. 5. All the terms in (37) in parentheses represent the disturbance terms due to the various cross-coupling effects between the d-q components as well as the rotor cross-coupling [1], [8], [9]. The leakages factors associated with these disturbances are:

$$\delta_1 = \frac{L_{mc}L_{mp}}{L_r L_{sp} - L_{mp}^2};\ \delta_2 = \frac{L_{mc}L_{sp}}{L_r L_{sp} - L_{mp}^2};\ \delta_3 = L_{sc} - \frac{L_{mc}^2 L_{sp}}{L_r L_{sp} - L_{mp}^2} \quad (38)$$

The disturbance associated with the derivative terms in (39) does not need to be included into the model because the controllers will be able to suppress them.

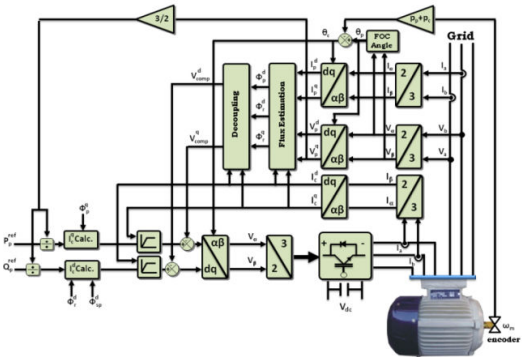

Fig. 5 Generator Side VSI FOC

In (37) is the presence of the PW stator flux and the rotor flux in as the control variables. We can't be measured directly of these quantities and would have to be estimated from the available voltage and current signals.

The reference frame is aligned with the d-component of the ψ_{sp}, the q-component (ψ_{sp}^q) always remains at zero [1], [8], [9]. The d-component of the PW stator flux is then calculated as:

$$\psi_{sp}^d = \frac{V_{sp}^q}{2\pi 50} \quad (39)$$

The rotor flux estimations are based on the knowledge of the PW and CW currents as well as PW flux in (35). By combining rotor flux expressions in (20)-(23) gives the estimated rotor flux in d-q reference frame:

$$\psi_r^q = \frac{L_{mp}^2 - L_{sp}L_r}{L_{mp}} i_{sp}^q + L_{mc} i_{sc}^q \quad (40)$$

$$\psi_r^d = \frac{L_{mp}^2 - L_r L_{sp}}{L_{mp}} i_{sp}^d + \frac{L_r}{L_{mp}}\psi_{sp}^d + L_{mc} i_{sc}^d \quad (41)$$

The reference signals i_{sc}^q and i_{sc}^d are obtained directly from the desired reactive and active powers command, respectively, by applying (42) and (43) to it.

$$i_{sc_{ref}}^d = \frac{P_{p_{ref}}}{1.5\, v_{sp}\, \delta_1} + \frac{\delta_4}{\delta_1}\psi_r^q \quad (42)$$

$$i_{sc_{ref}}^q = \frac{Q_{p_{ref}}}{1.5\, v_{sp}\, \delta_1} - \frac{\delta_5}{\delta_1}\psi_{sp}^d + \frac{\delta_4}{\delta_1}\psi_r^d \quad (43)$$

where

$$\delta_4 = \frac{L_{mp}}{L_r L_{sp} - L_{mp}^2}, \delta_5 = \frac{L_r}{L_r L_{sp} - L_{mp}^2} \quad (44)$$

V. Controller Design

In this section, we have chosen to compare the performances of the BDFIG with three different controllers.

A. PI Controller Synthesis

At present, the PI-type controller is most widely adopted in industrial application due to its simple structure [14], as shown in Fig. 6. Its control signal is easily computed by combining proportional-integral terms

$$u(t) = K_p e(t) + K_i \int e(t)\, dt \quad (45)$$

The terms K_p and K_i represent respectively the proportional and integral gains.

The quotient B/A represents the transfer function to be controlled, where A and B are presently defined as follows:

$$A = R_{sc} + s\,\delta_3 \; and \; B = 1 \quad (46)$$

where $\delta_3 = L_{sc} - \frac{L_{mc}^2 L_{sp}}{L_r L_{sp} - L_{mp}^2}$

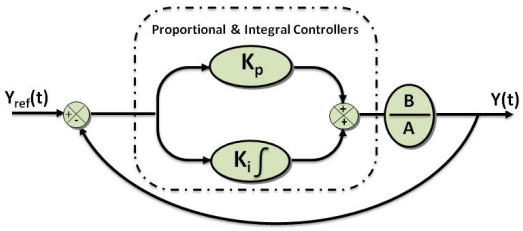

Fig. 6 System with PI controller

The controller terms can be calculated just specifying the natural frequency and damping of the close loop equivalent first order system. The desired natural frequency (ω_n) and damping (ξ) are set respectively to 37 rad/s and 70.7 %.

Allows determining the parameters of PI controller:

$$\begin{cases} K_i = \omega_n^2\, \delta_3 \cong 59 \\ K_p = 2\,\xi\,\omega_n\,\delta_3 - R_{sc} \cong 1.31 \end{cases} \quad (47)$$

The reason for the popular use of the PI-type controller is that this controller can be easily designed by adjusting only two controller parameters: K_p and K_i, [12], [14], [15]. In addition, its control performance can be accepted in many applications.

B. PD-Like Fuzzy Logic Controller Synthesis

The PD-like fuzzy logic controller (PD-like FLC) is driven by a set of control rules rather than constant proportional-derivative gains [11]-[16]. The block diagrams of a PD-like FLC, as shown in Fig. 7.

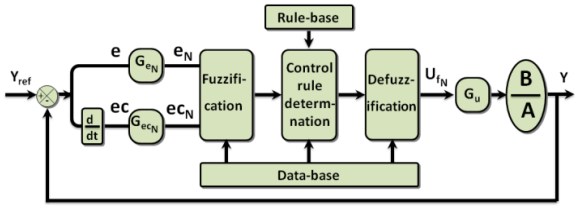

Fig. 7 Block diagram of PD-like Fuzzy Logic Controller

The PD-like FLC consists of four mechanisms: fuzzifier, fuzzy inferencing engine, knowledge base and a defuzzifier [15], [16], [18]. The input variables of PD-like FLC are the signals of error e(t) and rate of error change ec(t) and the output variable is generated from fuzzy rule base [12], [14]-[16]. After defuzzifier, the crisp signal is acquired.

The signals of error and error change are defined as

$$e(t) = I_{sc}^*(t_s) - I_{sc}(t_s) \quad (48)$$

$$ec(t_s) = e(t_s) - e(t_s - 1) \quad (49)$$

where $I_{sc}(t_s)$ is the actual stator current of CW and $I_{sc}^*(t_s)$ is the reference stator current of CW.

The inputs and the output are related as:

$$U_{fN}(t_s) = f\big(e(t_s), ec(t_s)\big) \quad (50)$$

The scaling factors G_{eN} and G_{ecN} are used to normalized error e(t) and error change ec(t) respectively, so that these remain within the limit of -1 to +1, and G_u is the gain of output scaling factor in the PD-like FLC [15], [16], [18]. This process of converting crisp variables into fuzzy variables is called fuzzification. After selecting the scaling factors, the next step is to choose the membership function for e(t), ec(t) and $U_f(t)$ [15], [16], [18]. The membership functions used for the input and output fuzzy set are shown in Fig. 8.

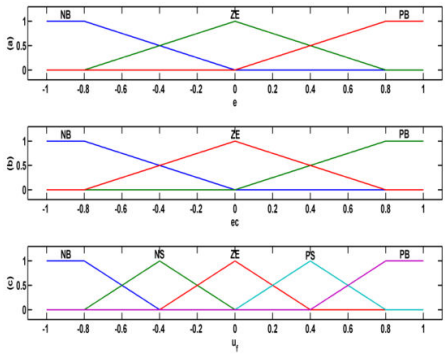

Fig. 8 Membership functions for: (a) error, (b) error change and (c) output U_f

The fuzzy inputs are inferred to a fuzzy rule base, which is used to characterize the relationship between fuzzy inputs and fuzzy output. In this study, the fuzzy rule base of PD-like FLC is fixed. It uses rules of the form, [15], [16], [18]:

R_{PD} : if e(t) is E(t) and ec(t) is EC(t) then $u_f(t)$ is U_F

The response of each fuzzy rule is weighted according to the degree of membership of its input conditions. After processing the inputs through knowledge base and inferencing mechanism the next stage is defuzzification [15], [16], [18]. In this paper, the defuzzification strategy chosen is the center average method [15], [16], [18]. Therefore, the output U_f can be computed as

$$U_{fN} = \frac{\sum_{k=1}^{n} u_{f(k)} \cdot \mu\left(u_{f(k)}\right)}{\sum_{k=1}^{n} \mu\left(u_{f(k)}\right)} \quad (51)$$

where n is the total number of rules and $\mu(U_f(k))$ denotes the output membership value for k^{th} rule.

The rule base of PD-like FLC is listed in Table I. Fig. 9 shows the output surface of output U_f

TABLE I
RULE BASE OF PD-LIKE FUZZY LOGIC CONTROLLER

ce \ e	NB	Z	PB
NB	NB	NS	Z
Z	NS	Z	PS
PB	Z	PS	PB

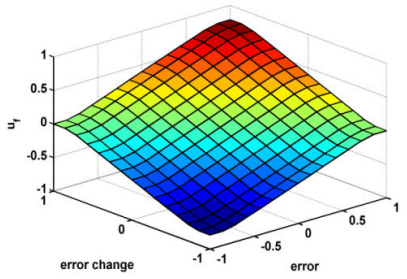

Fig. 9 Control surface of PD-like FLC (U_f)

C. The Proposed Controller–New Self Tuning fuzzy Proportional-Derivative Controller Synthesis

In order to improve the performance of the PD-like FLC controller, we propose a New Self-Tuning Fuzzy Proportional-Derivative Controller (NSTFPDC), is designed to tune the scaling factor of fuzzy output of control system. The block diagram of the proposed NSTFPDC is shown in Fig. 10.

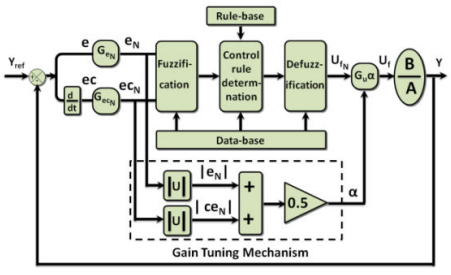

Fig. 10 Block diagram of NSTFPDC

The NSTFPDC has an output variable which is the gain-updating factor α, is applied to adjust the scaling factor of PD-like FLC output. All membership functions of the NSTFPDC inputs (e_N and ec_N) and the output (U_{fN}) are defined on the normalized domain [−1, 1], is not altered, as shown in Fig. 8. The rule base for computing controller output U_{fN} is shown above in Table I.

A practical observation of the generator step response, as shown in Fig. 11, is done. The current response can be roughly divided into four regions: $R_I - R_{IV}$, and two sets of particular points; crossover points (a_2, a_4) and peak points (a_3, a_5) are shown in Fig. 11 [11], [13], [15].

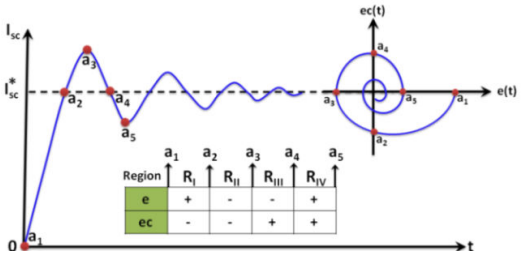

Fig. 11 Dynamic behavior of machine step response and mapping of response on e-ec state space

According to (48) and (49), the signs of e and ec will change when the response curve passes through the different regions. For example, the sign of e and ec in regions R_{II} and R_{IV} are (-, -) and (+, +), respectively [15], [16], [18]. The states in these two regions mean that the current now is not only upward R_{II} or downward R_{IV} far away from the current command but is also going farther away from it. In this case, the controller should provide large gain (αU_{fN}) to prevent worsening the condition [15], [16], [18]. This can be realized by the following rules:

If e is Negative and ec is Negative then αU_{fN} is Big.
If e is Positive and ec is Positive then αU_{fN} is Big.

When the states of the system are located on regions R_I and R_{III}, and the sign of e and ec is different. At this moment, the controller must make the gain Zero to evade overshoot and reduce the settling time [15], [16], [18]. The rule can be formed as follows:

If e is Negative and ec is Positive then αU_{fN} is Zero.
If e is Positive and ec is Negative then αU_{fN} is Zero.

In addition, when the state is located on the region of the steady state, i.e., each e or ec is zero, which means that the response has just reached or left the set point but is moving away upward or downward from the set point rapidly. In this situation, medium gain will prevent overshoot or undershoot [15], [16], [18]. This can be accomplished by the following rule:

If e is Zero and ec is Positive then αU_{fN} is medium.

If e is Zero and ec is Negative then αU_{fN} is medium.
If e is Positive and ec Zero is then αU_{fN} is medium.
If e is Negative and ec is Zero then αU_{fN} is medium.

Finally, at the steady state, the controller should provide zero gain to prevent the chattering problem around the set point [15], [16], [18]. The rule for this condition is as follows:

If e is Zero and ec is Zero then αU_{fN} is Zero.

As a result, based on the considerate and deduction of response behavior and the above rule base of αU_{fN}, we concluded that the output surface of gain-updating factor α is planned in Fig. 12.

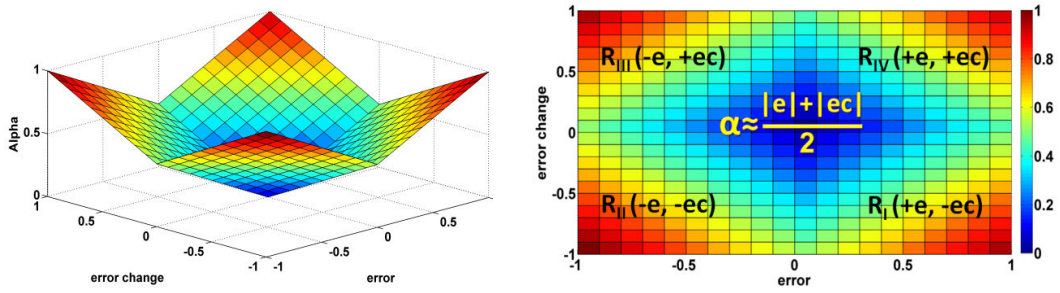

(a) (b)

Fig. 12 Proposed frame of the variation of gain updating factor (α) with error (e) and error change (ec)

Through Fig. 12 (b), we can deduce the single deterministic rule defined on the normalized of error (e) and change error (ce) as follows:

$$\propto = \frac{|e_N|+|ec_N|}{2} \tag{52}$$

The proposed heuristic rule is expected to improve the performance of the BDFIG in terms of reference tracking, sensibility to perturbations and parameters variations.

The relationship between scaling factors and the input and output variables of the controller are as follows:

$$e_N = G_{e_N} e \tag{53}$$

$$ec_N = G_{ec_N} ec \tag{54}$$

$$U_f = \propto G_u U_{fN} \tag{55}$$

Converting e, ec, and U_f into e_N, ec_N, and U_{fN} by the scaling gains, respectively, means that they are transferred from the actual discourse universe into the interval [−1, +1] (normalization) [15], [16]. The proper initial values are obtained when a good transient response is achieved

$$G_{eN} = \frac{1}{|I_{sc,max}|} \tag{56}$$

$$G_{ec_N} = \frac{1}{|\Delta I_{sc,max}|} \tag{57}$$

$$G_U = \Delta U_{f_{N,max}} \tag{58}$$

Comparative results for different controllers are presented below.

VI. Control of the Grid Inverter

The various control strategies for the voltage source rectifier (VSR) have been proposed [1], [17] and will be briefly discussed here.

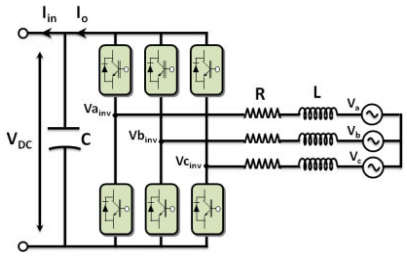

Fig. 13 VSR Circuit Model

The objective of the grid inverter is to maintain a constant DC-link voltage between BDFIG (CW) and grid.

The system can be described by the following equation [1],[17]:

$$\begin{bmatrix} V_a \\ V_b \\ V_c \end{bmatrix} = R \begin{bmatrix} i_a \\ i_b \\ i_c \end{bmatrix} + L \frac{d}{dt} \begin{bmatrix} i_a \\ i_b \\ i_c \end{bmatrix} + \begin{bmatrix} V_{a_{inv}} \\ V_{b_{inv}} \\ V_{c_{inv}} \end{bmatrix} \tag{59}$$

This can be written in a rotating reference frame by using Park transformation

$$\begin{bmatrix} V_q \\ V_d \end{bmatrix} = R \begin{bmatrix} i_q \\ i_d \end{bmatrix} + L \cdot s \begin{bmatrix} i_q \\ i_d \end{bmatrix} + \omega_e L \begin{bmatrix} i_q \\ -i_d \end{bmatrix} + \begin{bmatrix} V_{q_{inv}} \\ V_{d_{inv}} \end{bmatrix} \tag{60}$$

where s is the derivation operation.

$$\begin{cases} P = \frac{3}{2}(v_d i_d + v_q i_q) \\ Q = \frac{3}{2}(v_q i_d - v_d i_q) \end{cases} \tag{61}$$

The voltage components in the Park frame V_{d_inv} and V_{q_inv} are given at the output of the PI regulator:

$$\begin{cases} v_{d_{inv}} = -i_d(s\,L + R) + (\omega_e\,L\,i_q + v_d) \\ v_{q_{inv}} = -i_q(s\,L + R) + (\omega_e\,L\,i_d) \end{cases} \quad (62)$$

In the Park reference frame, the voltage source components are $V_d = 0$ and $V_q = V_s$ and the powers can be written as

$$\begin{cases} P = \frac{3}{2} v_q i_q \\ Q = \frac{3}{2} v_q i_d \end{cases} \quad (63)$$

By neglecting the converter losses, we have

$$\begin{cases} v_{dc} i_{dc} = \frac{3}{2} v_q i_q \\ C\frac{dv_{dc}}{dt} = i_{in} - i_o \end{cases} \quad (64)$$

$$v_{dc} C \frac{dv_{dc}}{dt} = P - P_m \quad (65)$$

The inner current loop can be modeled as a transfer function relating the terminal voltage and current

$$\frac{i(s)}{v(s)} = \frac{1}{L\,s + R} \quad (66)$$

The complete block diagram of the VSR controller is shown in Fig. 14 [1], [17].

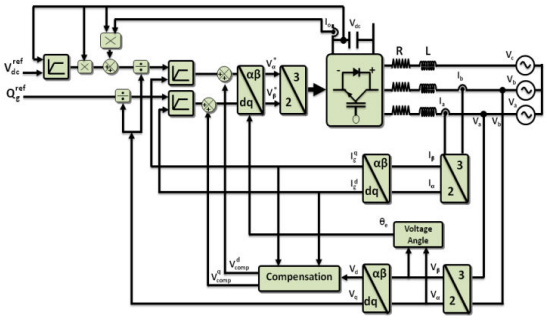

Fig. 14 Grid side VSR

VII. Simulation Results And Discussion

The aim of the control is to measure active and reactive powers equal to the reference values. These powers should then be collected in order to measure only the stator current of CW. The two controllers have been tested using the indirect control method. The method is based on the stator currents measurements of CW and gives then best results for the BDFIG control.

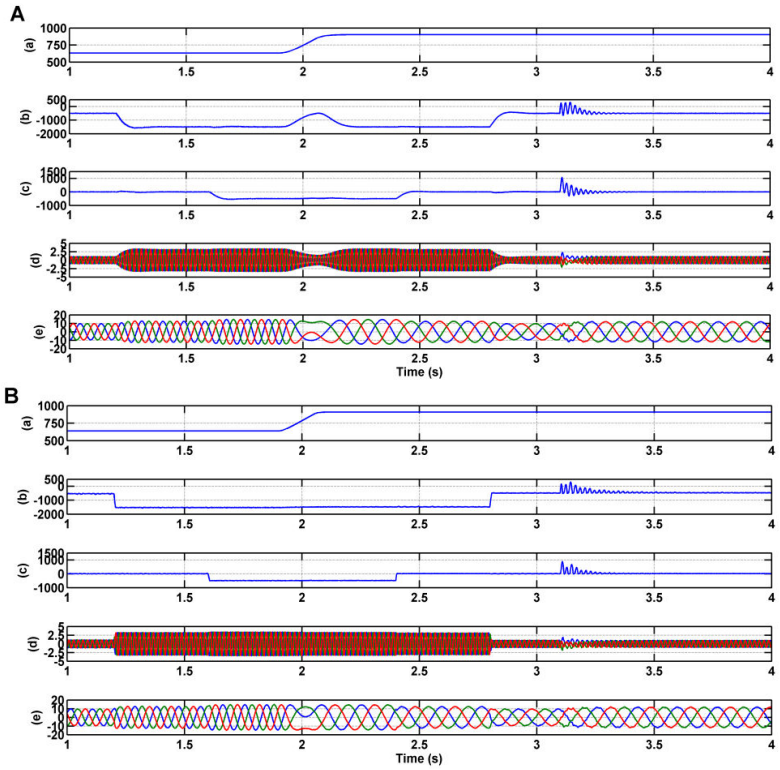

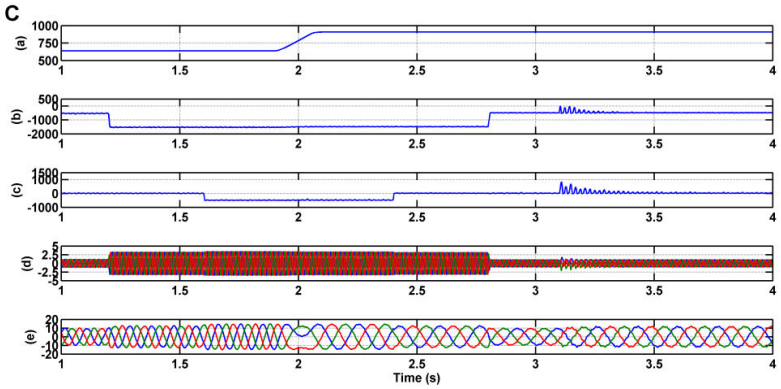

Fig. 15 Simulated results under various speed, stator reactive power steps and parameters variation (A) PI controller. (B) PD-like FLC Controller (C) NSTFPDC Controller; (a) Rotor speed (rmp). (b) Stator active power of PW (W). (c) Stator reactive power of PW (VAR). (d) Stator currents of PW (A). (e) Stator currents of CW (A)

A. Performances of the Controller

1. Reference Tracking

The first test investigated to compare the three controllers is reference tracking by applying stator active and reactive power steps of PW, respectively. As shown in Figs. 15 (b) and (c), the active power is stepped from -500 to -1.5 kW (export to grid) at 1.2 s and then backed to -500 at 2.8 s, the reactive power is stepped from 0 to -500 W at 1.6 s and then backed to 0 at 2.4 s, while the machine's speed is maintained constant during the first change at 640 rmp and at 910 rmp during the second change. The results are presented in Figs. 16 (a) and (b).

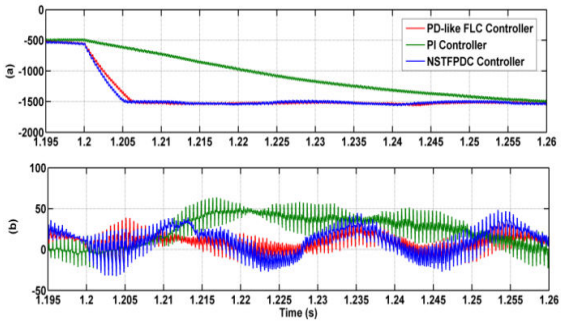

Fig. 16 Reference tracking, (a) Stator active power step of PW (b) Stator reactive power step of PW

Figs. 16 (a) and (b) showed that during the change of power, transient oscillations due to the coupling terms between the two axes and static error appear on active and reactive powers. This is inherent to the adopted control mode: the feedback signal of the controller is calculated using stator currents of CW and considering that stator resistance of CW is neglected. It can be seen that transient oscillations amplitude are minimized with NSTFPDC Controller which have better rejection of perturbations.

2. Sensibility to Perturbations

The aim of this test is to analyze the influence of a speed variation of the BDFIG on active and reactive powers. The active and reactive power references are maintained to −1.5 kW and -500 VAR and at time equal to 2 s the speed varies from 640 rmp to 910 rmp. The results are shown in Figs. 17 (a) and (b).

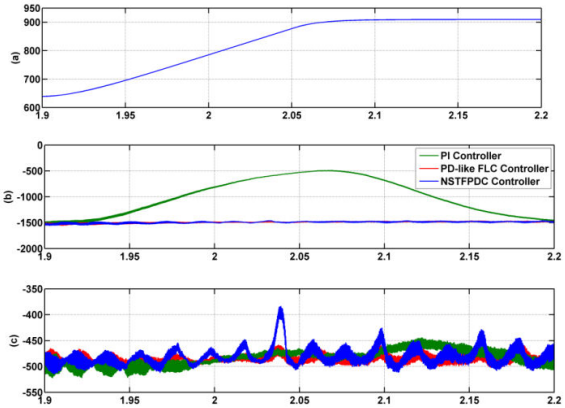

Fig. 17 Effect of a speed variation, (a) Rotor speed (rmp) (b) Stator active power step of PW (W) (c) Stator reactive power step of PW (VAR)

This figure shows the limits of the PI controller. Indeed, for this controller, a speed variation induces an important variation of the active and reactive powers (40% for active power and 2% for reactive power). PD-like FLC controller have lower than the previous values (2% for active power and 3% for reactive power) and the NSTFPDC Controller has a nearly perfect speed disturbance rejection, indeed, only small power variations can be observed (less than 1% for active power and 4% for reactive power). This result is interesting for wind energy applications to guarantee stability and quality of the generated power when the speed is varying.

3. Robustness

The aim of this test is to analyze the influence of the BDFIG's parameters variations on the controller's performances. The machine's model parameters have been deliberately modified with excessive variations: the values of

the both stators (PW and CW) and the rotor resistances are augmented by 25% and the values of inductances are reduced by 25%. The BDFIG is running at 910 rmp, active and reactive powers are maintained constant and the speed is equal to 910 rmp. The obtained results are presented in Figs. 18 (a) and (b).

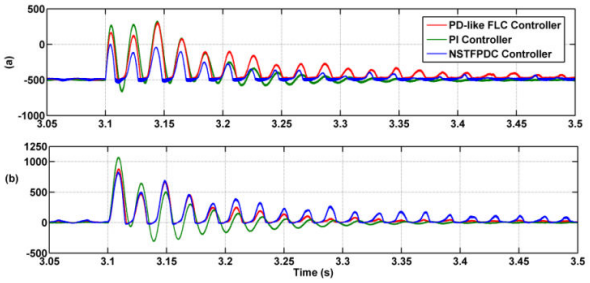

Fig. 18 Effect of BDFIG's parameters variation (a) Stator active power step of PW (W) (b) Stator reactive power step of PW (VAR)

These results show that parameters variations of the BDFIG increase the time-response of three Controllers, for the PI controller, parameters variations induces an important variation of the active and reactive powers (32% for active power and 42% for reactive power), PD-like FLC controller have lower than the previous values (24% for active power and 28% for reactive power), and NSTFPDC Controller is also have lower than the previous values (19% for active power and 26% for reactive power), Indeed, the transient oscillations due to the coupling terms between the two axes are always present for all controllers but their amplitudes have not been increased compared to the test with no parameters variation. However, a static error on reactive power appears when the value of the active power is changed but it keeps reasonable values.

B. Simulation of the Whole System

The wind energy system parameters used in the simulation are given as following:

TABLE II
WIND ENERGY SYSTEM PARAMETERS

Turbine	
	Diameter = 4.8 m, Number of blades = 3, Hub height = 12 m, Gearbox = 18
BDFIG [12]	
	2.6 Kw, 380 V, 50 Hz, 2 pole pairs, R_{sp} = 1.732 Ω, R_{sc} = 1.079 Ω, R_r = 0.473Ω, L_{sp} = 714.8 mH, L_{sc}= 121.7 mH, L_{mp}=242.1 mH, L_{mc}=59.8 mH. L_r = 132.6 mH.
filter	
	Z_f =R +jLω = 0.25 +j0.003.

Fig. 19 shows the wind speed. Fig. 20 shows the angular speed random of the BDFIG. Fig. 21 presents the decoupling effect between the direct and quadratic stator flux of PW. The stator currents and voltages waveforms of the BDFIG and the related expended plots are shown, respectively, in Figs. 22 (a), (b), (c), and (d) (phase a). The PWM inverters are operated at 2 kHz; hence, the currents are almost sinusoidal. The stator currents (PW and CW) waveforms and these zoom are presented, correspondingly, in Figs. 23 (a) and (b). Fig. 24 gives the rotor current of the BDFIG. The stator active and reactive powers are plotted in Fig. 25. Fig. 26 shows the regulation of the DC-link voltage. It is maintained at a constant level (410 V) so that the real power extracted from the wind energy conversion system can pass through the grid.

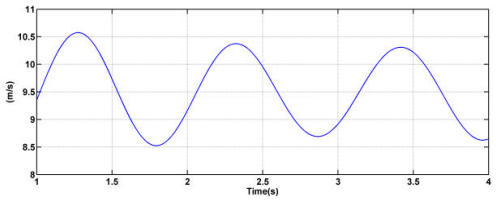

Fig. 19 wind speed (V_w)

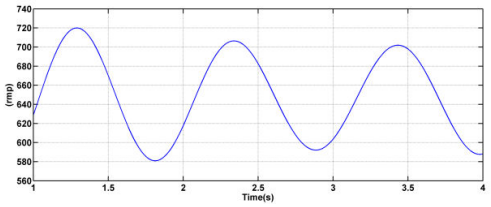

Fig. 20 Random of the BDFIG rotor speed (Ω_{mec})

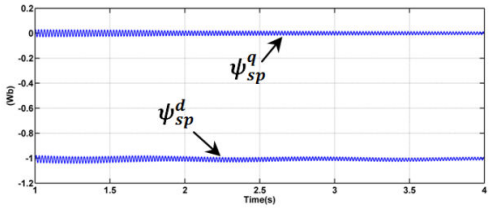

Fig. 21 Direct and quadratic stator flux of PW (ψ^{q}_{sp} and ψ^{d}_{sp})

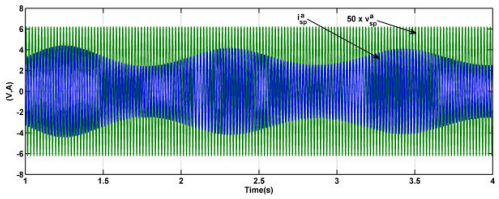

Fig. 22 (a) Stator current and voltage of PW (I^{a}_{sp}, V^{a}_{sp})

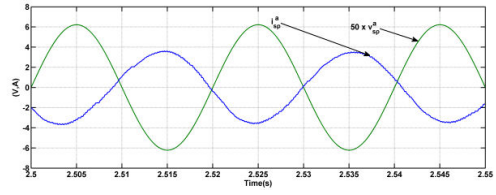

Fig. 22 (b) Zoom of Stator current and voltage of PW (I^{a}_{sp}, V^{a}_{sp})

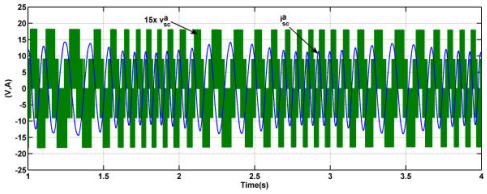

Fig. 22 (c) Stator current and voltage of CW (I_{sc}^{a}, V_{sc}^{a})

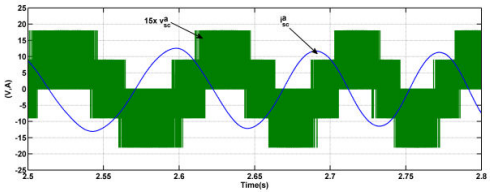

Fig. 22 (d) Zoom of Stator current and voltage of CW (i_{sc}^{a}, v_{sc}^{a})

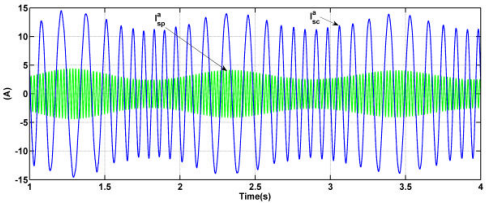

Fig. 23 (a) Stator currents of PW and CW (i_{sc}^{a}, i_{sp}^{a})

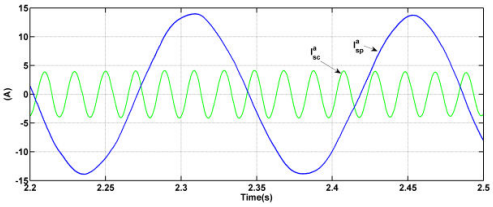

Fig. 23 (b) Zoom of Stator currents of PW and CW (i_{sc}^{a}, i_{sp}^{a})

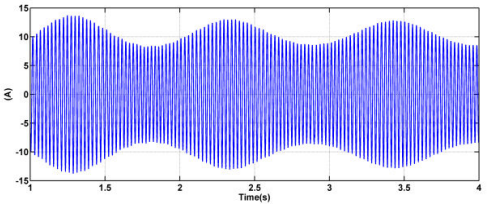

Fig. 24 Rotor current (i_{r}^{a})

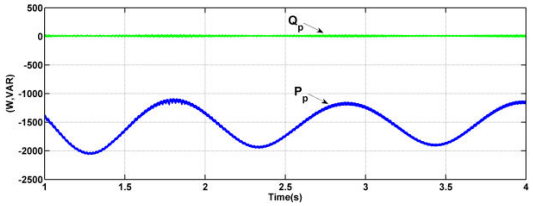

Fig. 25 Stator active and reactive powers (P_p, Q_p)

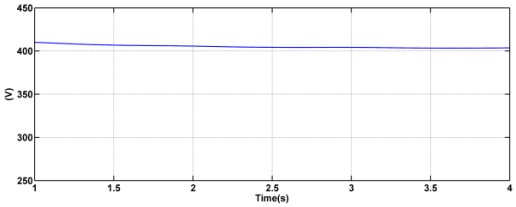

Fig. 26 DC-link voltage (E)

VIII. Conclusions

In this paper, a New Self-Tuning Fuzzy Proportional-Derivative Controller (NSTFPDC) has been proposed and associated to the oriented control field of a brushless doubly fed induction generator based wind energy conversion systems connected to the grid.

In this paper, we have presented a complete system to produce electrical energy with a BDFIG by the way of a wind turbine. Three different controllers (PI, PD-like FLC and NSTFPDC) are synthesized and compared. In terms of power, reference tracking with the BDFIG.

The presented results show that a new technique for the intelligent control method as NSTFPDC can be a very attractive solution for devices using BDFIG such as wind energy conversion systems.

Nomenclature

The turbine

Ω_{mec}	Mechanical speed of the BDFIG
Ω_t	Turbine speed
Ω_{mec_ref}	Mechanical speed reference
P_t	Mechanical power
P_{mec_ref}	Mechanical power optimal
C_{aer}	Aerodynamic torque
C_g	Generator torque
C_p	Power coefficient
λ	Tip speed ratio
ρ	Air density
R	Turbine radius
V_w	Wind velocity
G	Gear ratio
S	cross-sectional area
J_t	Inertia
F_t	Viscous friction

The BDFIG

$v_{sp}^{q}, v_{sp}^{d}, v_{sc}^{q}, v_{sc}^{d},$	"d-q" stators voltages
$i_{sp}^{q}, i_{sp}^{d}, i_{sc}^{q}, i_{sc}^{d}$	"d-q" stators currents
$\psi_{sp}^{q}, \psi_{sp}^{d}, \psi_{sc}^{q}, \psi_{sc}^{d}$	"d-q" stators flux
i_{r}^{q}, i_{r}^{d}	"d-q" rotor currents
N_r	Number of rotor nests
R_{sp}, R_{sc}	Per phase stators resistances
R_r	Per phase rotor resistance
L_{sp}, L_{sc}	Total cyclic stators inductances
L_r	Total cyclic rotor inductance
L_{mp},L_{mc}	Magnetizing inductances
p	Number of pole pairs
S	derivative operator
J_g	inertia

F_g	viscous friction
C_{em}	electromagnetic torque
P_{sp}, Q_{sp}	active and reactive stator powers
P_g, Q_g	active and reactive grid powers
ω_e	speed of the reference frame
ω_p, ω_c,	stators synchronous angular frequency
ω_r	rotor's electrical angular speed
ω_m	rotor's mechanical angular speed

REFERENCES

[1] K. Protsenko and D. Xu, "Modeling and control of brushless doubly fed induction generators in wind energy applications," in Proc. APEC Conference, 2007.
[2] S. El-Aimani, "Modélisation de différentes technologies d'éoliennes intégrées dans un réseau de moyenne tension," Univ. des Sciences et Technologies de Lille, Thèse de Doctorat, Dec. 2004.
[3] A.K. Wallace, R. Spee and G.C. Alexander, "The brushless doubly-fed machine: its advantages, applications and design methods," in proc. 6th Inte. Conf. on EMD, 1993.
[4] S.WiIliamson, A.C. Ferreira and A.K. Wallace, "Generalised theory of the brushless doubly-fed machine. Part I: Analysis," IEE Proc. Electr. Power Appl., Vol. 144, Mar. 1997, pp. 111-122.
[5] P. C. Roberts," A study of brushless doubly-fed (induction) machines," Thesis of PhD, University of Cambridge, 2004.
[6] R.A. McMahon, P.C. Roberts, X. Wang and P.J. Tavner, "Performance of BDFM as generator and motor," IEE Proc. Electr. Power Appl., Vol. 153, Mar. 2006, pp. 289-299.
[7] J. Poza, E. Oyarbide, I. Sarasola, M. Rodriguez, "Unified reference frame dq model of the brushless doubly fed machine," IEE Proc. Electr. Power Appl., Vol. 153, Sep. 2006, pp. 726-734.
[8] J. Poza, E. Oyarbide, I. Sarasola, M. Rodriguez, "Vector control design and experimental evaluation for the brushless doubly fed machine," IET Electr. Power Appl, Vol. 3, 2009, pp. 247–256.
[9] S. Shao, E. Abdi, F. Barati and R. McMahon, "Stator-fux-oriented vector control for brushless doubly fed induction generator," IEEE Trans. Ind. Electro., Vol. 56, 2009, pp. 4220-4228.
[10] I. Sarasola, J. Poza, M. A. Rodriguez and G. Abad, "Direct torque control design and experimental evaluation for the brushless doubly fed machine," Journal of ECM, Vol. 52, 2011, pp. 1226-1234.
[11] C. C. Lee, "Fuzzy logic in control systems fuzzy logic controller, Part I and Part II" IEEE Trans. On Syeteme. MAN. And Cybernetics, vol. 20, Mar./Apr. 1990, pp. 404-418.
[12] J. Lee, "On methods for improving performance of pi-type fuzzy logic controllers," IEEE Trans. on fuzzy systems, vol. 1, Nov. 1993, pp. 298-301.
[13] H. X. Li and H. B. Gatland, "A new methodology for designing a fuzzy logic controller," IEEE Trans. on systems, man, and cybernetics, vol. 25, Mar. 1995, pp. 505-512.
[14] R. K. Mudi and N. R. Pal, "A robust self-tuning scheme for PI- and PD-type fuzzy controllers," IEEE Trans. on fuzzy systems, vol. 7, Feb. 1999, pp. 2-16.
[15] S. C. Wang and Y. H. Liu, "A modified PI-like fuzzy logic controller for switched reluctance motor drives," IEEE Trans. On industrial electronics, vol. 58, may 2011, pp. 1812-1825.
[16] R. R. De, R. K. Mudi and A. K. Pal, "A PD-type self-tuning FLC for second-order systems with dead-time," in Proc. ICACCCT, 2012, pp. 409-413.
[17] R. Pena, J.C. Clare and G. M. Asher, "Doubly fed induction generator using back-to-back PWM converters and its application to variable speed wind-energy generation," IEE Proc. Electr. Pow. Appl., Vol. 143, 1996, pp. 231–241.
[18] G. Feng, "A survey on analysis and design of model-based fuzzy control systems," IEEE Trans. on fuzzy systems, vol. 14, Oct 2006, pp. 676-697.
[19] E. Merabet, H. Amimeur, F. Hamoudi and R. Abdessemed, "Self–tuning fuzzy logic controller for a dual star induction machine," Journal of Electrical Engineering & Technology, Vol. 6, Jan. 2011, pp. 133-138.
[20] K. Protsenko "Flexible power flow control for brushless doubly fed induction generator," Thesis of M.Sc, Ryerson University, 2003.
[21] M. Yamamoto and O. Motoyoshi, "Active and reactive power control for doubly-fed wound rotor induction generator," IEEE Trans. on Power Elecronics., VOL 6, Oct. 1991, pp. 624-629.
[22] Y. Tang and L. Xu, "A flexible active and reactive power control strategy for a variable speed constant frequency generating system," IEEE Trans. On Power Electronics, Vol. 10, July. 1995, pp. 472-478.